

# Molecular nature of the $a_1(1260)$ axial-vector meson

Samson Clymton<sup>1,\*</sup> and Hyun-Chul Kim<sup>1,2,†</sup>

<sup>1</sup>*Department of Physics, Inha University, Incheon 22212, Republic of Korea*

<sup>2</sup>*School of Physics, Korea Institute for Advanced Study (KIAS), Seoul 02455, Republic of Korea*

We investigate  $\pi\rho$  scattering based on the coupled-channel formalism with the  $\pi\rho$  and  $K\bar{K}^*$  ( $\bar{K}K^*$ ) channels included. We construct the kernel amplitudes by using the meson-exchange model and compute the coupled integral equation for  $\pi\rho$  scattering. By performing the partial-wave expansion, we show explicitly that the  $a_1(1260)$  meson is dynamically generated by the coupled-channel formalism. The  $a_1$  meson only appears by including the  $K\bar{K}^*$  ( $\bar{K}K^*$ ) channel. We obtain the pole position of the  $a_1$  meson as  $\sqrt{s_R} = (1170.1 - i104.1)$  MeV. We conclude that the  $a_1$  meson can be interpreted as a kaon and vector kaon molecular state.

*Introduction.* – The  $a_1(1260)$  meson is the first axial-vector meson. If chiral symmetry  $SU(2) \otimes SU(2)$  is unbroken, then the  $\rho$  and  $a_1$  mesons form a chiral doublet [1, 2] as the  $\pi$  and  $\sigma$  ( $f_0(500)$ ) do. The existence of the  $a_1$  meson has been well established since the ACCMOR Collaboration [3] confirmed it in partial wave analyses of the  $\pi^-\pi^-\pi^+$  system. However, the values of its mass and width do not reach an experimental consensus. For example, the ARGUS Collaboration at DESY [4] found the mass of the  $a_1$  meson to be  $m_{a_1} = (1046 \pm 11)$  MeV and its width to be  $\Gamma_{a_1} = (521 \pm 27)$  MeV in the decay  $\tau \rightarrow \pi^-\pi^-\pi^+\nu_\tau$  whereas the CLEO Collaboration announced a rather large values  $m_{a_1} = (1331 \pm 10 \pm 3)$  MeV and  $\Gamma_{a_1} = (814 \pm 36 \pm 13)$  MeV in the decay  $\tau \rightarrow \pi^-\pi^0\pi^0\nu_\tau$  [5]. Recently, the LHCb Collaboration measured  $m_{a_1} = (1195.050 \pm 1.045 \pm 6.333)$  MeV and  $\Gamma_{a_1} = (422.013 \pm 2.096 \pm 12.723)$  MeV in  $D^0 \rightarrow K^\mp\pi^\pm\pi^\pm\pi^\mp$  decays [6]. Moreover, one should keep in mind that there is an inevitable model dependence in analyzing the experimental data. The Particle Data Group (PDG) estimates the average values of the  $a_1$  mass and width as  $m_{a_1} = (1230 \pm 40)$  MeV and  $\Gamma_{a_1} = (420 \pm 35)$  MeV.

Since the  $a_1$  meson has quantum numbers as  $J^{PC} = 1^{++}$ , it can be constructed as  $q\bar{q}$  ( $1^3P_1$ ) state. It is an isovector meson with negative  $G$  parity. Dankowych et al. [7] carried out the isobar-model partial-wave analysis of high statistics data on  $\pi^-p \rightarrow \pi^+\pi^-\pi^0n$  from the Argonne National Laboratory zero-gradient synchrotron. They extracted the partial-wave cross section of  $\pi\rho$  scattering in S and D waves. The  $a_1$  resonance was observed in the S-wave cross section with the broad width, which reaches the kaon and vector kaon ( $\bar{K}K^*$ ) threshold. It was even seen that the  $a_1$  meson decays into  $\bar{K}$  and  $K^*$  [5, 8, 9]. It implies that the  $a_1$  meson may be strongly coupled to the  $K$  and  $K^*$ . Thus, the  $a_1$  meson may contain the tetraquark component, or it can even be interpreted as the molecular state [10–13]. A similar situation can be found in the case of the scalar-isovector meson  $a_0(980)$ , which is often interpreted either as a tetraquark state or as a resonance appearing from the  $\pi\eta$  and  $K\bar{K}$  coupled channels [14–17]. The scalar mesons  $f_0(500)$  and  $f_0(980)$  meson are also considered as the tetraquark or molecular states [16, 18–22]. In particular, the  $f_0(980)$  is just below the  $K\bar{K}$  threshold, it can be regarded as a  $K\bar{K}$  molecular state [19, 23].

Janssen et al. [24] constructed the meson-exchange model for  $\pi\rho$  scattering with the effective Lagrangian, including the  $a_1$  meson explicitly. In the present work, we will extend the work of Ref. [24] by considering the coupled-channel formalism. We add the  $K\bar{K}^*$  ( $\bar{K}K^*$ ) channel to the  $\pi\rho$  channel but exclude the  $a_1$  meson. We will show how the  $K\bar{K}^*$  ( $\bar{K}K^*$ ) channel generates dynamically the  $a_1$  meson and describe successfully the S-wave cross section. We first formulate the kernel amplitude based on the meson-exchange model. We treat the vector meson based on the hidden local gauge symmetry [25, 26]. This has a certain merit that the coupling constants are constrained. Then we solve the coupled integral equation for  $\pi\rho$  scattering. The results for the S-wave cross section clearly reveals the  $a_1$  meson with a broad width. We find the pole position in the second Riemann sheet as  $\sqrt{s_R} = (1170.1 - i104.1)$  MeV.

*General formalism* – We start from the definition of the scattering amplitude expressed as

$$\mathcal{S}_{fi} = \delta_{fi} - i(2\pi)^4 \delta^4(P_f - P_i) \mathcal{T}_{fi}, \quad (1)$$

where  $P_f$  and  $P_i$  denote the total four-momenta of the final and initial state. The formal transition amplitude  $\mathcal{T}_{fi}$  is obtained from the Bethe-Salpeter (BS) equation with the coupled-channel formalism employed:

$$\mathcal{T}_{fi}(p', p; s) = \mathcal{V}_{fi}(p', p; s) + \frac{1}{(2\pi)^4} \int d^4q \mathcal{V}_{fk}(p', q; s) \mathcal{G}_k(q; s) \mathcal{T}_{ki}(q, p; s), \quad (2)$$

\* E-mail: sclymton@inha.edu

† E-mail: hchkim@inha.ac.kr

where  $s$  is the square of the total energy.  $p$ ,  $p'$  and  $q$  stand respectively for the four-momenta of the initial, final and intermediate mesons in the center of mass (CM) frame. The indices  $i$  and  $f$  represent the initial and final meson channels, and  $k$  designates the intermediate state in the coupled-channel formalism. Since it is rather complicated to deal with the BS equation, we use its three-dimensional reduction, which is not unique. In the current work, we utilize the Blankenbecler-Sugar (BbS) equation [27, 28] that preserves the unitarity of two-body interaction for all energies and keeps Lorentz invariance. It is convenient to introduce the coupled-channel formalism and is expressed as

$$\mathcal{T}_{fi}(\mathbf{p}', \mathbf{p}; s) = \mathcal{V}_{fi}(\mathbf{p}', \mathbf{p}; s) + \frac{1}{(2\pi)^3} \int \frac{d^3q}{2E_{k1}(\mathbf{q})E_{k2}(\mathbf{q})} \mathcal{V}_{fk}(\mathbf{p}', \mathbf{q}; s) \frac{E_k(\mathbf{q})}{s - E_k^2(\mathbf{q})} \mathcal{T}_{ki}(\mathbf{q}, \mathbf{p}; s), \quad (3)$$

where  $E_{ki} = (\mathbf{q}^2 + m_{ki})^{1/2}$  and  $E_k = E_{k1} + E_{k2}$ . The zeroth component of the momenta is determined by the propagator  $\mathcal{G}_k$  given as  $q_0 = (E_{k1} - E_{k2})/2$ .

Since we are mainly interested in the  $a_1$  meson, we need to consider only the two channels:  $\pi\rho$  and  $K\bar{K}^*$  ( $\bar{K}K^*$ ) ones. Other channels such as the  $\pi\omega$  and  $\pi\phi$  do not contribute to the production of the  $a_1$  meson. In the coupled-channel formalism, the kernel  $\mathcal{V}_{fi}$  in Eq. (3) is expressed as

$$\mathcal{V}_{fi} = \begin{pmatrix} \mathcal{V}_{\pi\rho \rightarrow \pi\rho} & \mathcal{V}_{K\bar{K}^* \rightarrow \pi\rho} \\ \mathcal{V}_{\pi\rho \rightarrow K\bar{K}^*} & \mathcal{V}_{K\bar{K}^* \rightarrow K\bar{K}^*} \end{pmatrix}, \quad (4)$$

where the off-diagonal part of  $\mathcal{V}_{fi}$  contains the transition from  $\pi\rho \rightarrow K\bar{K}^*$  ( $\bar{K}K^*$ ). Since  $K$  and  $K^*$  have no definite  $G$ -parity, we need to combine the  $K\bar{K}^*$  and  $\bar{K}K^*$  states, which gives a state with the definite  $G$  parity:

$$|K\bar{K}^*(\pm)\rangle = \frac{1}{\sqrt{2}} (|K\bar{K}^*\rangle \pm |\bar{K}K^*\rangle). \quad (5)$$

Note that we consider only the negative one because  $\pi\rho$  has negative  $G$ -parity. We will see later that the  $K\bar{K}^*$  channel with the positive  $G$ -parity decouples from the  $\pi\rho$  channel.

The kernel  $\mathcal{V}_{fi}$  in Eq. (4) is modeled by meson-exchange diagrams as drawn generically in Fig. 1. Since the  $a_1$

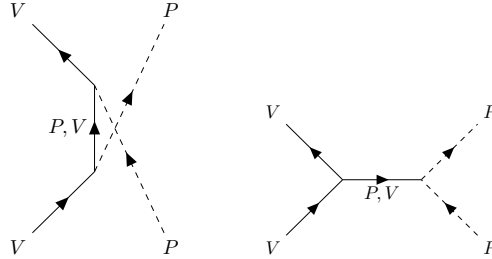


FIG. 1. The  $t$ - (left) and  $u$ -channels (right) of the meson-exchanged diagrams.

meson will be dynamically generated by the coupled-channel formalism, we do not include it in the  $s$  channel. The vertices in the Feynman diagrams are formulated from the SU(3) symmetric effective Lagrangians given by

$$\begin{aligned} \mathcal{L}_{PPV} &= g_{PPV} \text{Tr}([P, \partial_\mu P] V^\mu), \\ \mathcal{L}_{VVV} &= -\frac{1}{2} g_{VVV} \text{Tr}((\partial_\mu V_\nu - \partial_\nu V_\mu) V^\mu V^\nu), \\ \mathcal{L}_{PVV} &= \frac{g_{PVV}}{m_V} \varepsilon^{\mu\nu\alpha\beta} \text{Tr}(\partial_\mu V_\nu \partial_\alpha V_\beta P), \end{aligned} \quad (6)$$

where subscripts  $V$  and  $P$  denote the vector and pseudoscalar mesons involved in the vertices.  $m_V$  represents the mass of the vector meson. We choose  $g_{PPV} = g_{VVV}$  by regarding the vector mesons as dynamical gauge bosons arising from hidden local gauge symmetry. We fix the coupling constants by setting  $a = 2$  [25, 26]. The values of the coupling constants are taken from Ref. [24]:  $g_{PPV}^2/4\pi = 0.71$  and  $g_{PVV}^2/4\pi = 1.88$ . However, since flavor SU(3) symmetry is broken, the coupling constants vary from the SU(3) symmetric case. When it is necessary, we change the values of the coupling constants, which are not far from the SU(3) symmetric ones, so that we can fit the experimental data. However, we regard the  $\phi$ -exchange coupling constant as a free parameter. Its value we have selected differs from the SU(3) symmetric one by 14%. As for the propagators of the exchange mesons, we utilize the static ones, following Ref. [24].

The trace operators in Eq. 6 run only over flavor space. The matrices for the pseudoscalar and vector mesons are expressed respectively as

$$P = \begin{pmatrix} \frac{1}{\sqrt{2}}\pi^0 + \frac{1}{\sqrt{6}}\eta & \pi^+ & K^+ \\ \pi^- & -\frac{1}{\sqrt{2}}\pi^0 + \frac{1}{\sqrt{6}}\eta & K^0 \\ K^- & \bar{K}^0 & -\frac{2}{\sqrt{6}}\eta \end{pmatrix}, \quad (7)$$

$$V_\mu = \begin{pmatrix} \frac{1}{\sqrt{2}}\rho_\mu^0 + \frac{1}{\sqrt{2}}\omega_\mu & \rho_\mu^+ & K_\mu^{*+} \\ \rho_\mu^- & -\frac{1}{\sqrt{2}}\rho_\mu^0 + \frac{1}{\sqrt{2}}\omega_\mu & K_\mu^{*0} \\ K_\mu^{*-} & \bar{K}_\mu^{*0} & \phi_\mu \end{pmatrix}. \quad (8)$$

where we employ the standard mixing for the  $\omega_1$  and  $\omega_8$  components such that the  $\omega$  meson contains only the  $u$  and  $d$  quarks whereas the  $\phi$  meson only comprises the strange quark. We ignore the  $\eta'$  meson for this study. The flavor part of Eq. 6 can be evaluated in the isospin bases and yield factors labeled as IS listed in the fourth column of Table I. From Table I, we find it obvious that the positive  $G$ -parity of  $K\bar{K}^*$  channel cannot be coupled to the  $\pi\rho$  channel.

TABLE I. The factor IS for all possible exchange diagram for each reaction. Note that the value inside the parentheses is given for the conjugate state of  $K\bar{K}^*$ .

Reaction	Exchange	Type	IS
$\pi\rho \rightarrow \pi\rho$	$\pi$	$u$	4
	$\rho$	$t$	-4
	$\omega$	$u$	-4
$\pi\rho \rightarrow K\bar{K}^*(\bar{K}K^*)$	$K$	$u$	-2(2)
	$K^*$	$t$	2(-2)
$K\bar{K}^* \rightarrow K\bar{K}^*$	$\rho$	$t$	1
	$\omega$	$t$	-1
	$\phi$	$t$	-2
$K\bar{K}^* \rightarrow \bar{K}K^*$	$\pi$	$u$	1
	$\eta$	$u$	-3
	$\rho$	$u$	-1
	$\omega$	$u$	1
	$\phi$	$u$	2

Since hadron has a finite size, we introduce a form factor at each vertex. We use the following parametrization for the form factors

$$F(t) = \left( \frac{n\Lambda^2 - m^2}{n\Lambda^2 - t} \right)^n, \quad F(u) = \left( \frac{n\Lambda^2 - m^2}{n\Lambda^2 - u} \right)^n, \quad (9)$$

where  $m$  denotes the mass of the exchange particle.  $n$  is determined by the power of momentum in the vertex. For example, we take  $n = 1$  for the VPP vertex whereas we choose  $n = 2$  for the VVP one. Though the cut-off masses  $\Lambda$  are free parameters, we reduce the uncertainties by fixing their values as follows: we add (600 – 700) MeV to the exchange mass. This idea is based on the fact that a heavier particle has a smaller size [29, 30]. Thus, the value of  $\Lambda$  is also taken to be larger than that of the corresponding meson mass by around (600 – 700) MeV. To fit the data, however, we choose a larger value of the cut-off mass especially for  $\phi$  exchange, where its value is 1700 MeV higher than that of the exchanged meson mass. In addition, we drop out the energy and angular dependence of the form factors for the sake of simplicity [24].

Since the  $a_1$  meson arises from the S-wave transition amplitude, we carry out the partial wave decomposition of the kernel and transition amplitudes. The partial-wave helicity amplitudes can be obtained by projecting the amplitudes onto the total angular momentum  $J$

$$\mathcal{T}_{\lambda'\lambda}^{J(fi)}(\mathbf{p}', \mathbf{p}) = \mathcal{V}_{\lambda'\lambda}^{J(fi)}(\mathbf{p}', \mathbf{p}) + \frac{1}{(2\pi)^3} \sum_{g, \lambda_g} \int \frac{q^2 dq}{2E_{k1}(q)E_{k2}(q)} \mathcal{V}_{\lambda'\lambda_g}^{J(fg)}(\mathbf{p}', \mathbf{q}) \frac{E_k(q)}{s - E_k^2(q)} \mathcal{T}_{\lambda_g\lambda}^{J(gi)}(\mathbf{q}, \mathbf{p}), \quad (10)$$

where  $\lambda'$ ,  $\lambda$  and  $\lambda_g$  denote the helicities of the final ( $f$ ), initial ( $i$ ) and intermediate ( $g$ ) state, respectively. The partial-wave kernel amplitudes can be expressed as

$$\mathcal{V}_{\lambda'\lambda}^{J(fi)}(\mathbf{p}', \mathbf{p}) = 2\pi \int d(\cos\theta) d_{\lambda'\lambda}^J(\theta) \mathcal{V}_{\lambda'\lambda}^{fi}(\mathbf{p}', \mathbf{p}, \theta), \quad (11)$$

where  $\theta$  denotes the scattering angle and  $d_{\lambda'\lambda}^J(\theta)$  stand for the matrix elements of the Wigner  $D$  functions. The partial-wave  $\mathcal{T}$  amplitude is also expressed in a similar manner.

The partial-wave coupled integral equation in Eq. (10) is solved numerically after we regularize the singularity arising from the two-body meson propagator  $\mathcal{G}$ . We build the matrix  $\mathcal{V}$  in the momentum space, containing both the  $\pi\rho$  and  $K\bar{K}^*$  channels. Then  $\mathcal{T}$  matrix can be derived by the Haftel-Tabakin's method of the matrix inversion [31]

$$\mathcal{T} = \left(1 - \mathcal{V}\tilde{\mathcal{G}}\right)^{-1} \mathcal{V}. \quad (12)$$

It is convenient to write the  $\mathcal{T}$  matrix in the particle basis [32]. Thus, we define  $\mathcal{T}_{IJL}$  as the  $\mathcal{T}$  matrix for given total isospin  $I$ , total angular momentum  $J$ , and orbital angular momentum  $L$ .

*$a_1$  meson as a  $K\bar{K}^*$  molecular state* – We discuss now how the  $a_1$  meson can be dynamically generated by the coupled channel formalism. In Fig. 2, we draw the real part of  $\mathcal{T}_{110}$  in  $K\bar{K}^* \rightarrow K\bar{K}^*$  reaction. This channel corresponds

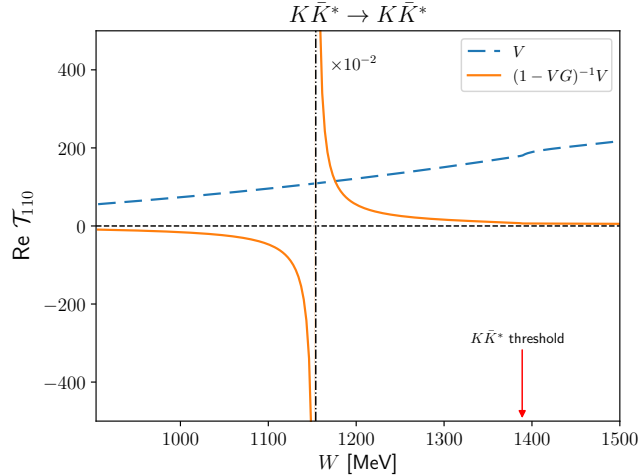


FIG. 2. Real part of  $\mathcal{T}_{110}$  in the  $K\bar{K}^* \rightarrow K\bar{K}^*$  reaction as a function of energy. The dashed line depicts it when  $\mathcal{V}$  is only considered whereas the solid curve draws it when  $(1 - \mathcal{V}\mathcal{G})^{-1}\mathcal{V}$  is solved.

to the quantum number of the  $a_1$  resonance. The kernel amplitude  $\mathcal{V}$  itself does not show any resonance behavior, which is depicted as the dashed line. On the other hand, the full transition amplitude generates the singularity below the  $K\bar{K}^*$  threshold energy after the integral equation is solved. Note that this singular behavior in  $\mathcal{T}$  is responsible for creating the  $a_1$  meson in the  $\pi\rho \rightarrow \pi\rho$  reaction. The remarkable point is that it only appears below the  $K\bar{K}^*$  threshold.

To compared the experimental data [7] given in an arbitrary unit, one can take the total cross section to be

$$\sigma \equiv \sigma_{\pi\rho}(t = m_\rho^2, M_{\pi\rho}) = -C \text{Im}[\mathcal{T}_{\pi\rho}(M_{\pi\rho})], \quad (13)$$

where  $C$  is the constant to match the data to the results from a theoretical model. Figure 3 shows the result for  $\sigma$  as a function of the  $\pi\rho$  invariant mass. The solid curve draws the current result whereas the dot-dashed one corresponds to that from Ref. [24] in which the  $a_1$  meson was explicitly introduced as a  $s$ -channel pole diagram with the  $\pi\rho$  channel only. The result from Ref. [24] shows a symmetric shape, since the  $a_1$  pole diagram governs it. On the other hand, the present result reveals a dynamical feature. It describes well the experimental data on  $\pi\rho$  scattering near the  $\pi\rho$  threshold. The S-wave total cross section rapidly increases and reaches the maximum value at around 1150 MeV. The current work explains the  $\pi\rho$  cross section but the maximum value is shifted to the higher value of  $m_{\pi\rho}$ . While the result from Ref. [24] falls off rapidly, so that it is underestimated in the vicinity of the  $K\bar{K}^*$  threshold, the present result decreases slowly. It describes well the data near the  $K\bar{K}^*$  threshold. If we turn off the  $K\bar{K}^*$  channel, the result cannot yield the  $a_1(1260)$  resonance structure at all. Thus, The  $K\bar{K}^*$  channel plays a critical role in generating the  $a_1$  resonance. A similar situation can be found in the case of the  $f_0(980)$  meson. In Ref. [19],  $\pi\pi$  scattering was investigated within the meson-exchange model, where the  $f_0(980)$  resonance can only appear when the  $K\bar{K}$  channel was included. A similar feature was also observed in Ref. [23]. So, the  $f_0(980)$  meson is often considered as a  $K\bar{K}$  molecular state.

To scrutinize the  $a_1(1260)$  resonance based on the current work, we evaluate the pole position for this resonance in the second Riemann sheet and coupling strength at the pole position. We locate the pole position  $a_1$  at  $\sqrt{s_R} =$

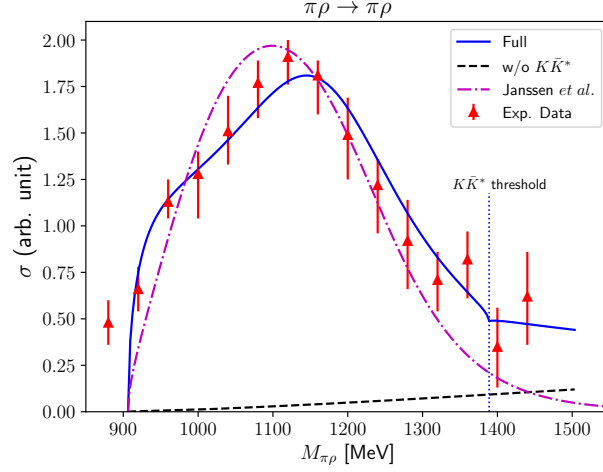


FIG. 3. Comparison of the  $\pi\rho \rightarrow \pi\rho$  total cross section for  $IJL = 110$  as a function of  $\pi\rho$  invariant mass with that from Ref. [24]. The solid curve draws the result from the present work whereas the dot-dashed one depicts that from Ref. [24]. The dashed line exhibits the result with the  $K\bar{K}^*$  channel turned off. The experimental data are taken from Ref. [7].

(1170.1 - i104.1) MeV in the complex energy plane. Since there is no other resonance nearby, we can determine clearly its position. From the pole position we found, we obtain the smaller width of the  $a_1$  meson compared to that from Ref. [7], where  $\Gamma = (380 \pm 100)$  MeV was obtained by using the Bowler model fit. However, if we carefully analyze our work, there is a threshold enhancement and the effect from opening the  $K\bar{K}^*$  channel, which make the peak structure broader.

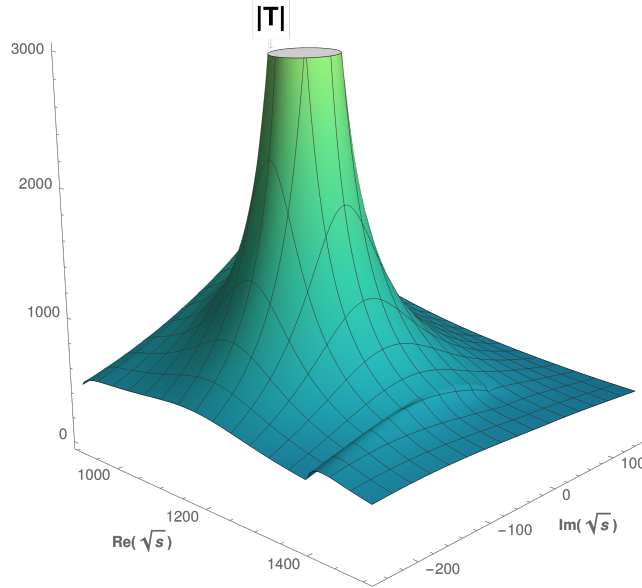


FIG. 4. The 3D plot of absolute  $T$  matrix as a function of complex energy.

To see the  $a_1$  resonance structure more explicitly, we also present the 3D plot of the  $|T|$  in the complex energy plane, as illustrated in Fig. 4. To derive the coupling strengths of the  $a_1$  meson coupled to the  $\pi\rho$  and  $K\bar{K}^*$  channels, we derive it from the residue of the transition amplitude defined as  $\mathcal{R}_{a,b}$ :

$$\mathcal{R}_{a,b} = \lim_{s \rightarrow s_R} (s - s_R) \mathcal{T}_{a,b}. \quad (14)$$

The coupling strengths are defined as the square root of the residue of the transition amplitude, so that we obtain

them as

$$g_{\pi\rho}^{a_1} = \sqrt{\mathcal{R}_{\pi\rho,\pi\rho}^{a_1}} = 5.20 - i0.63 [\text{GeV}], \quad (15)$$

$$g_{K\bar{K}^*}^{a_1} = \sqrt{\mathcal{R}_{K\bar{K}^*,K\bar{K}^*}^{a_1}} = 6.11 - i0.39 [\text{GeV}]. \quad (16)$$

Note that we choose the positive signs for both coupling strengths, since we are not able to determine them.

*Conclusions* – In the present work, we studied  $\pi\rho$  scattering based on the meson-exchange model, focusing on the  $a_1(1260)$  resonance appearing in the S-wave total cross section. We showed that the coupled-channel formalism including the  $\pi\rho$  and  $K\bar{K}^*$  channels generated the  $a_1$  meson dynamically. The  $K\bar{K}^*$  channel plays an essential role in producing the  $a_1$  meson. We obtained the pole position of the  $a_1$  resonance at  $\sqrt{s_R} = (1170.1 - i104.1) \text{ MeV}$ . The present result is much better than the previous one that was obtained by considering the  $\pi\rho$  single channel with the  $a_1$  meson included explicitly as the  $s$ -channel pole diagram. We also derived the coupling strengths  $g_{\pi\rho}^{a_1}$  and  $g_{K\bar{K}^*}^{a_1}$  from the residue of the transition amplitude. These results imply that the dynamically generated  $a_1$  meson may be interpreted as a  $K\bar{K}^*$  molecular state.

*Acknowledgments* – The present work was supported by Basic Science Research Program through the National Research Foundation of Korea funded by the Korean government (Ministry of Education, Science and Technology, MEST), Grant-No. 2021R1A2C2093368 and 2018R1A5A1025563.

- 
- [1] S. Weinberg, Precise relations between the spectra of vector and axial vector mesons, Phys. Rev. Lett. **18**, 507 (1967).
  - [2] M. Gell-Mann and M. Levy, The axial vector current in beta decay, Nuovo Cim. **16**, 705 (1960).
  - [3] C. Daum *et al.* (ACCMOR), Experimental proof of the existence of the A1 meson, Phys. Lett. B **89**, 281 (1980).
  - [4] H. Albrecht *et al.* (ARGUS), Measurement of tau decays into three charged pions, Z. Phys. C **33**, 7 (1986).
  - [5] D. M. Asner *et al.* (CLEO), Hadronic structure in the decay  $\tau \rightarrow \nu_\tau \pi^- \pi^0 \pi^0$  and the sign of the tau-neutrino helicity, Phys. Rev. D **61**, 012002 (2000), arXiv:hep-ex/9902022.
  - [6] R. Aaij *et al.* (LHCb), Studies of the resonance structure in  $D^0 \rightarrow K^\mp \pi^\pm \pi^\pm \pi^\mp$  decays, Eur. Phys. J. C **78**, 443 (2018), arXiv:1712.08609 [hep-ex].
  - [7] J. A. Dankowych *et al.*, Evidence for  $I = 1(A1)$  and  $I = 0(H)$  axial vector resonances in charge exchange, Phys. Rev. Lett. **46**, 580 (1981).
  - [8] A. Drutskoy *et al.* (Belle), Observation of  $B \rightarrow D^* K^- K^{0*}$  decays, Phys. Lett. B **542**, 171 (2002), arXiv:hep-ex/0207041.
  - [9] T. E. Coan *et al.* (CLEO), Wess-Zumino current and the structure of the decay  $\tau \rightarrow K^- K^+ \pi^- \nu_\tau$ , Phys. Rev. Lett. **92**, 232001 (2004), arXiv:hep-ex/0401005.
  - [10] J. L. Basdevant and E. L. Berger, Unitary coupled-channel analysis of diffractive production of the  $a_1$  resonance, Phys. Rev. D **16**, 657 (1977).
  - [11] L. Roca, E. Oset, and J. Singh, Low lying axial-vector mesons as dynamically generated resonances, Phys. Rev. D **72**, 014002 (2005), arXiv:hep-ph/0503273.
  - [12] M. F. M. Lutz and E. E. Kolomeitsev, On meson resonances and chiral symmetry, Nucl. Phys. A **730**, 392 (2004), arXiv:nucl-th/0307039.
  - [13] H. Nagahiro, K. Nawa, S. Ozaki, D. Jido, and A. Hosaka, Composite and elementary natures of  $a_1(1260)$  meson, Phys. Rev. D **83**, 111504 (2011), arXiv:1101.3623 [hep-ph].
  - [14] R. L. Jaffe, Multi-quark Hadrons. 1. The phenomenology of (2 quark 2 anti-quark) mesons, Phys. Rev. D **15**, 267 (1977).
  - [15] N. N. Achasov, S. A. Devyanin, and G. N. Shestakov, Is There a 'Signature' of the  $\delta$  (980) meson four quark nature?, Phys. Lett. B **96**, 168 (1980).
  - [16] V. Baru, J. Haidenbauer, C. Hanhart, Y. Kalashnikova, and A. E. Kudryavtsev, Evidence that the  $a_0(980)$  and  $f_0(980)$  are not elementary particles, Phys. Lett. B **586**, 53 (2004), arXiv:hep-ph/0308129.
  - [17] Z.-Q. Wang, X.-W. Kang, J. A. Oller, and L. Zhang, Analysis on the composite nature of the light scalar mesons  $f_0(980)$  and  $a_0(980)$ , Phys. Rev. D **105**, 074016 (2022), arXiv:2201.00492 [hep-ph].
  - [18] D. Lohse, J. W. Durso, K. Holinde, and J. Speth, Scalar Mesons in  $\pi\pi$  and  $K\pi$  Scattering, Phys. Lett. B **234**, 235 (1990).
  - [19] D. Lohse, J. W. Durso, K. Holinde, and J. Speth, Meson exchange model for pseudoscalar meson meson scattering, Nucl. Phys. A **516**, 513 (1990).
  - [20] C. Amsler and N. A. Tornqvist, Mesons beyond the naive quark model, Phys. Rept. **389**, 61 (2004).
  - [21] H. A. Ahmed and C. W. Xiao, Study the molecular nature of  $\sigma$ ,  $f_0(980)$ , and  $a_0(980)$  states, Phys. Rev. D **101**, 094034 (2020), arXiv:2001.08141 [hep-ph].
  - [22] N. N. Achasov, J. V. Bennett, A. V. Kiselev, E. A. Kozyrev, and G. N. Shestakov, Evidence of the four-quark nature of  $f_0(980)$  and  $f_0(500)$ , Phys. Rev. D **103**, 014010 (2021), arXiv:2009.04191 [hep-ph].
  - [23] J. A. Oller and E. Oset, Chiral symmetry amplitudes in the S wave isoscalar and isovector channels and the  $\sigma$ ,  $f_0(980)$ ,  $a_0(980)$  scalar mesons, Nucl. Phys. A **620**, 438 (1997), [Erratum: Nucl. Phys. A 652, 407–409 (1999)], arXiv:hep-ph/9702314.

- [24] G. Janssen, K. Holinde, and J. Speth, A meson exchange model for  $\pi$   $\rho$  scattering, Phys. Rev. C **49**, 2763 (1994).
- [25] M. Bando, T. Kugo, S. Uehara, K. Yamawaki, and T. Yanagida, Is rho meson a dynamical gauge boson of hidden local symmetry?, Phys. Rev. Lett. **54**, 1215 (1985).
- [26] M. Bando, T. Kugo, and K. Yamawaki, On the vector mesons as dynamical gauge bosons of hidden local symmetries, Nucl. Phys. B **259**, 493 (1985).
- [27] R. Blankenbecler and R. Sugar, Linear integral equations for relativistic multichannel scattering, Phys. Rev. **142**, 1051 (1966).
- [28] R. Aaron, R. D. Amado, and J. E. Young, Relativistic three-body theory with applications to  $\pi^- n$  scattering, Phys. Rev. **174**, 2022 (1968).
- [29] J.-Y. Kim and H.-C. Kim, Electromagnetic form factors of singly heavy baryons in the self-consistent SU(3) chiral quark-soliton model, Phys. Rev. D **97**, 114009 (2018), arXiv:1803.04069 [hep-ph].
- [30] J.-Y. Kim, H.-C. Kim, G.-S. Yang, and M. Oka, Electromagnetic transitions of the singly charmed baryons with spin 3/2, Phys. Rev. D **103**, 074025 (2021), arXiv:2101.10653 [hep-ph].
- [31] M. I. Haftel and F. Tabakin, Nuclear saturation and the smoothness of nucleon-nucleon potentials, Nucl. Phys. A **158**, 1 (1970).
- [32] R. Machleidt, K. Holinde, and C. Elster, The Bonn meson exchange model for the nucleon nucleon Interaction, Phys. Rept. **149**, 1 (1987).